GLOBAL INSTABILITY ANALYSIS OF A ROUND JET

Shintaro TAKEUCHI*
Department of Mechanical Engineering, Osaka University
2-1 Yamadaoka, Suita, Osaka, Japan
shintaro@fluid.mech.eng.osaka-u.ac.jp

Yutaka MIYAKE
Department of Mechanical Engineering, Osaka University
2-1 Yamadaoka, Suita, Osaka, Japan
miyake@mech.eng.osaka-u.ac.jp

ABSTRACT

In order to investigate the diversity of the evolution of near-field of a round jet observed in experiments and in numerical simulations by different authors, the secondary stability is analyzed which appears in the early stage of spatial development of a round jet in its near field. The secondary instability which is characterized by generation of streamwise vortices in a braid region between neighbouring vortex rings is analyzed by a global instability analysis. Unstable modes of disturbances are identified by the analysis in a base flow of an axial segment of one pitch of a round jet between one pair of vortex rings. The linear bound of their evolution as well as the interaction of each mode are investigated by introducing these disturbances on the base flow. The key of the role of these disturbances in the spatial evolution of a round jet is examined by introducing modes into the baseflow and the wavelet analysis, etc. It turned out that the most probable cause of the diversity of the evolution is a non-uniform concentration of disturbances in the azimuthal direction, which is dependent on environmental disturbances and hence non-deterministic. This non-uniformity looks like a result of delicate local receptivity of disturbance.

INTRODUCTION

Lots of studies on a round jet have been conducted and the flow looks like almost completely understood except for the near flield of a round jet which is particulary important in engineering applications. For instance, the distance of virtual origin from the nozzle exit scatters pretty largely between authors. The manner of the scatter is not consistent and no persuasive reasoning has been given to this. In addition, complicated phenomena which are beyond our understing are also found. An example is that the speed of the temporal development of streamwise vortices which connects the region between neighbouring vortex rings(a braid region) fluctuates with time(Takeuchi et al, 1999), despite that time-averaged speed of its development is approximately that of the least stable mode of disturbance in a braid region.

The major concern here is whether the scatter of the speed of collapse in the near field is inherent and substantially unavoidable or not, if all the predictable source of the scatter is carefully removed. This problem is treated here from the view point of the secondary instability which takes place succeeding the primary instability. Since the flow field is pretty distorted non-parallel flow in the secondary instability process, an analytical treatment of an instability problem is often difficult. In the present work, a global instability analysis based on large scale numerical simulation is employed. The mechanism of the non-uniform concentration and resulting different temporal growth rate of streamwise vortices in a braid region in the secondary instability process is discussed based on the stability analysis.

BASE FLOW

For the present global instability analysis, temporally developing jet which is periodic in axial direction is used as the baseflow. The computational domain is a cylinder of an axial length $\ell/D = 2\pi/5$ and the radius $R/D = 6$ where D is the diameter of the centerline of a ring vortex. The axial length corresponds

*Research Fellow of the Japan Society for the Promotion of Science

to the most unstable wavenumber $\alpha = 5$ of the primary instability stage for the axi-symmetric parallel flow of a round jet with uniform core covered with boundary layer of momentum thickness $\Theta/D = 0.045$ of its peripfery. At the initial stage of the reproduction of a base-flow, the parallel flow is excitated at the axial wavenumber $\alpha = 5$ to accomodate a pair of vortex rings in the computational domain. In the calculation, the vortex ring does not always stay at the edge of computational domain, but slowly moves to downstream at the speed of the phase velocity of the most unstable mode in the primary instability regime. The grid number is (64,64,128) in axial(z),radial(r) and circumferential(θ) directions, respectively. Reynolds number based on U_0, the core velocity and D is 25000.

CALCULATION METHOD

Suppose the baseflow $\boldsymbol{u}(\boldsymbol{v}, p)$ where $\boldsymbol{u}$ and p is velocity and pressure respectively, is an N-dimensional vector which obeys the Navier-Stokes equation $d\boldsymbol{u}/dt = \boldsymbol{f}$, where N-dimensional vector $\boldsymbol{f}$ contains convective, pressure and viscous terms. A small disturbance vector $\boldsymbol{u'}(\boldsymbol{v'}, p', t)$ superposed on the baseflow follows the linearized N-S equation:

$$\frac{d\boldsymbol{u'}}{dt} = A\boldsymbol{u'} \qquad \text{where } A = \frac{\partial \boldsymbol{f}}{\partial \boldsymbol{u'}} . \qquad (1)$$

Assuming exponential growth of the perturbation with time t as $\boldsymbol{u'} = \tilde{\boldsymbol{u}} e^{\lambda t}$, Eq.(1) is written in the following form:

$$A\tilde{\boldsymbol{u}} = \lambda \tilde{\boldsymbol{u}} . \qquad (2)$$

which is an eigen equation.

On the other hand, time integration of Eq.(1) from t to $t+T$ yields

$$\tilde{\boldsymbol{u}}(\boldsymbol{v'}, p', t+T) = B_T \tilde{\boldsymbol{u}}(\boldsymbol{v'}, p', t) \quad \text{where } B_T = e^{AT} . \qquad (3)$$

where T is within the regime in which the base flow grows linearly. By the theorem of Frobenius concerning matricial polynomial, eigenvalues λ, λ_b of A, B_T are connected with each other by $\lambda_b = \mathrm{e}^{\lambda T}$. As the exponential transformation (3) keeps the eigenvectors of A and B_T identical, Eq.(2) is transformed into

$$B_T \tilde{\boldsymbol{u}} = \lambda_b \tilde{\boldsymbol{u}} \qquad \text{where } \lambda_b = e^{\lambda T} \qquad (4)$$

by time-integration. In 3-dimensional flow analysis, the dimension N of A, B_T and $\tilde{\boldsymbol{u}}$ could attain as huge as $10^5 \sim 10^7$ corresponding to the grid number, each of which has pressure and 3 components of velocities. As eigenvalue problem of this huge size asymmetric matrix is too big to solve directly as it is, an approximate but efficient method should be introduced. The technique proposed by Eriksson and Rizzi (1985) extended from the Arnoldi's method (Arnoldi, 1951) allows us to reduce the size of matrix. The outline of the present global instability analysis based on these techniques is described briefly in the following.

Let E_N represent the vector space spanned by whole eigenvectors of A, B_T and let $\boldsymbol{\zeta}_j$ be the normalized disturbance vector obtained by an orthogonalization of $B_T \boldsymbol{\zeta}_i$ to every ingredient of the set of vectors $\boldsymbol{\zeta}_1, \cdots, \boldsymbol{\zeta}_{j-1}$. $M (M \ll N)$ sets of these orthonormal vectors $V_M = \{\boldsymbol{\zeta}_1, \cdots, \boldsymbol{\zeta}_M\}$ constitute the orthonormal basis in the subspace E_M of E_N(Takeuchi, 2001), which may allow us to approximate the eigenvector $\boldsymbol{\varphi} \in E_M$ of A and B_T as the linear combination of $\boldsymbol{\zeta}_i$'s as follows:

$$\boldsymbol{\varphi} = z_1 \boldsymbol{\zeta}_1 + z_2 \boldsymbol{\zeta}_2 + \cdots + z_M \boldsymbol{\zeta}_M = V_M \, \boldsymbol{z} \qquad (5)$$

where $\boldsymbol{z} = \{z_1, \cdots, z_M\}^T$ is the coefficient vector. Expecting that $\boldsymbol{\varphi}$ is close enough to the correct eigenvector $\tilde{\boldsymbol{u}}$ in Eq.(4), approximate eigenvalue λ_b is obtained as the solution of

$$V_M^T B_T V_M \, \boldsymbol{z} = \lambda_b \boldsymbol{z}, \quad (\text{where } V_M^T V_M = I) \qquad (6)$$

where I is an unit matrix of dimension N. As the matrix $V_M^T B_T V_M$ is an M-dimensional square matrix, Eq.(6) is much smaller in dimension than the original eigenvalue problem of Eq.(2) and (4). Then, λ obtained by inverse-transform of λ_b by Eq.(4) and the corresponding vector $V_M \boldsymbol{z}$ represent the approximate eigenvalue and eigenvector of A, respectively. Positive eigenvalues make the system (1) temporally unstable.

Direct solution of $V_M^T A V_M \boldsymbol{z} = \lambda \boldsymbol{z}$ is also possible for eigensystem of A, in principle. However, solution of Eq.(6) achieves better accuracy at reduced dimension $M (\ll N)$ for unstable modes which satisfy $0 < \lambda < \lambda_b$, particularly as the magnitude of eigenvalue $|\lambda|$ increases (Saad,1980 and Takeuchi,2001).

RESULTS

In this calculation, reduced dimension M for the global instability analysis is 200, in place of the original dimension of $N = 2.5 \times 10^5$ which is the number of grid points used for flow simulation. Time interval T in Eq.(3) is 5 in non-dimensional time which corresponds to the time length for a vortex ring to advect about 2ℓ. As will be mentioned later,

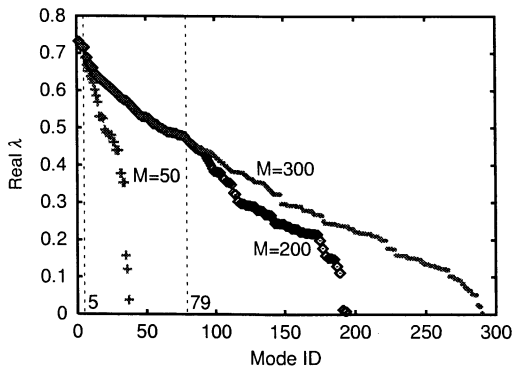

Figure 1: Eigenvalue λ of the secondary instability arranged in the descending order of Real[λ], for $M = 50(+)$, $M = 200(\diamond)$ and $M = 300(\bullet)$.

Table 1: Number of set of streamwise ribs of Fig.2 aligned in the circumferential direction. Each set of ribs is composed of a positive and a negative streamwise vortices.

Mode No.	01	04	08	11	24	34
Num. of ribs	4	5	6	7	13	18

unstable modes in the secondary instability evolve linearly in this interval of T in the currently assumed baseflow. Figure 1 shows the magnitude of the real part of the eigenvalue λ. Three cases of $M = 50, 200$ and 300 are shown to demonstrate the accuracy. Eigenvalues are arranged in the descending order of Real[λ]. It is noted that analysis of the case of $M = 200$ gives enough accurate solution up to 79th largest eigenvalue in comparison with $M = 300$ case. It is also found that no dominant mode exist but amplification rates of neighbouring modes are very close in magnitude with each other. The magnitude of first several modes are within 2.5% of the largest one which is 0.73. Figure 2 shows examples of the eigenvectors corresponding to several typical unstable modes, visualized by iso-surfaces of positive streamwise vorticity $|\boldsymbol{\omega}| = 4$ (dark iso-surface) along with the baseflow (bright iso-surface). Modes' ID number corresponds to the order of Real[λ] in Fig.1. Between neighbouring positive streamwise vortices there is a negative streamwise vortex which is similar in shape to positive ones, though not shown in the figure to simplify the visualization. In the first mode (Mode01), four sets of streamwise vortices bridge the outer edge of the upstream vortex ring and inner edge of the downstream one, spanning braid region. The number of pairs of streamwise vortices of typical unstable modes shown in Figs.2(a)$\sim$(f) are tabulated in Table1. According to Fig.1, corresponding eigenvectors obtained at $M = 200$ coincide

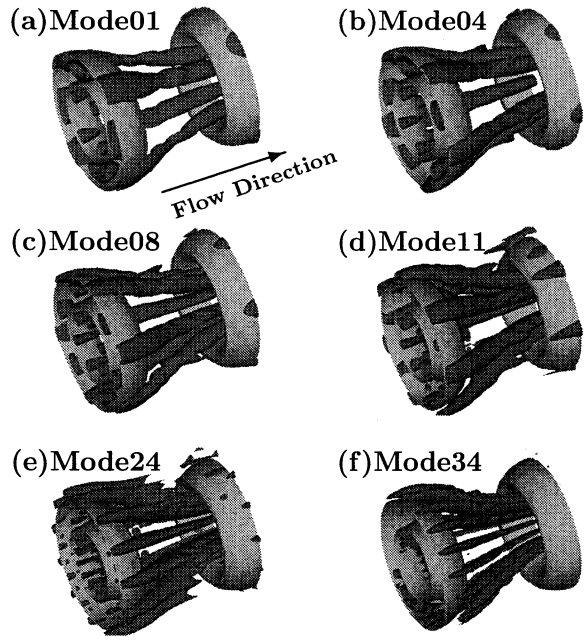

Figure 2: Typical unstable perturbations represented by iso-surface of positive streamwise vorticity(dark iso-surface) together with the baseflow(bright iso-surface) as $|\omega| = 4$.

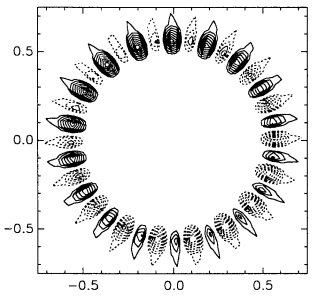

Figure 3: Contour of streamwise vorticity of Mode34. Solid line : positive, Dotted line : negative.

with those obtained at $M = 300$ within error of 1×10^{-9}, where the error between two eigenvectors $\boldsymbol{s}$ and $\boldsymbol{t}$ is defined by $(1 - \frac{\boldsymbol{s}}{|\boldsymbol{s}|} \cdot \frac{\boldsymbol{t}}{|\boldsymbol{t}|})$. Vortical structures of unstable modes in Figs.2 are rotationally symmetric in the circumferential direction except for Mode34 which is rotationally asymmetric. Fig.3 shows the contour of streamwise vorticity ω_z in the cross-section in the braid of Mode34. Streamwise vorticity ω_z is weakly varying in azimuthal direction and its phase overturns in a half circle.

LINEARITY OF UNSTABLE MODES

To confirm linear bound of the temporal development of perturbations in a braid region, the growth of the above-selected perturbations in Fig.2 are calculated by superposing

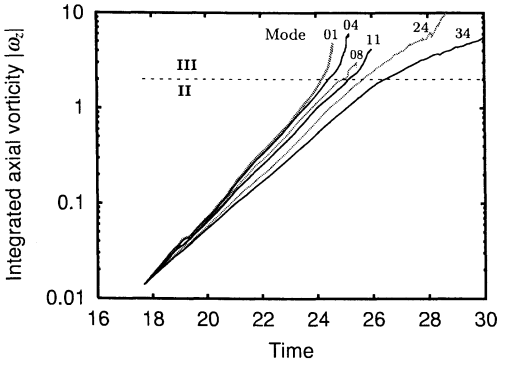

Figure 4: Temporal growth of unstable modes in Figs.2 superposed on the baseflow.

the modes on the baseflow. Superposed mode consists of pressure and 3 components of velocity and the specified initial kinetic energy is $1.5 \times 10^{-3}\%$ of that of the base flow. Figure 4 shows temporal growth of the integrated axial vorticity $I \equiv \int_S |\omega_z| dS$ measured in the mid cross-section S between the neighbouring ring vortices, where the section S is chased as the vortex ring moves to axial direction, identifying the point of slowest centerline velocity as the detector.

Each mode grows linearly until it reaches the break-up. The temporal growth rate given by the gradient of each curve is same as Real[λ] in Fig.1, which confirms the accuracy of the present global instability analysis. After the secondary perturbation grows up to the threshold of $I \simeq 2$, the growth rate of each mode changes. As will be mentioned later, chaotic vortices look dominant in the flow field beyond this threshold. The breakdown of the secondary stage indicated by crossing this threshold is referred hereafter as the tertiary instability. This threshold also corresponds to the upper bound of the secondary instability regime. The onset of the break-up of the tertiary instability is in the order of the magnitude of eigenvalue, as expected.

In order to investigate the dependence of temporal growth on initial intensity of unstable modes, similar simulations have been conducted with different initial intensity of unstable modes. As a result, temporal growth rate of I of each mode and the onset of the tertiary instability are the same as in Fig.4. The property of additivity of unstable modes has been confirmed also by comparing the evolved perturbations started from sum of unstable modes with that obtained by summing each independently evolved perturbations. The evolution is done within the linear bound and the difference between them is as small as 0.0006 in the

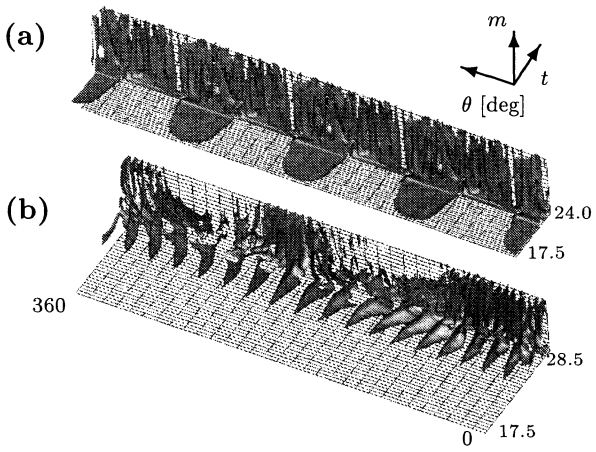

Figure 5: Temporal evolution of the wavelet signals of (a)Mode01 and (b)Mode34. Initial intensities are set to be the same as that in Fig.4.

earlier mentioned definition of difference.

Consequently, unstable modes obtained by the global instability analysis possess the linearity in the secondary instability regime.

THE ANALYSIS OF NON-UNIFORMITY IN UNSTABLE MODES

In this section, temporal evolution of vortical structure of unstable modes is described. For this, ω_z distribution is adopted as the indicator. First, to see the difference between the evolution of two basically different disturbance modes, Mode01 and Mode 34 are independently superposed on the base flow. The former is the representative of rotationally symmetric mode and the latter, that of rotationally asymmetric one. Temporal evolution of each mode is analyzed. The wavelet transform (Chui, 1992) is applied to streamwise vorticity ω_z on a circle of radius $r = D/2$ in a cross-section S in a braid region which moves to downstream as time goes on. The wavelet transform is conducted by using the Morlet's wavelet as a mother wavelet in the azimuthal direction.

The obtained time series of wavelet signal are depicted in three-dimensional manner as $W_\psi \omega_z(m, \theta, t)$ in Fig.5, ordinary two-dimensional wavelet map of wavenumber(m) of ω_z and azimuthal angle(θ) are arranged along t-axis. Figs.5(a),(b) are the 3-D wavelet maps for Mode01 and 34 as in Fig.2, respectively.

The front-end of t-axis is at $t = 17.5$ in both Fig.2(a) and (b), when small amplitude disturbances are introduced. The timeseries demonstrate temporal evolution of streamwise

vorticity from the very beginning to final stage through the secondary up to the tertiary instability process at $t = 28.5$ in (a) and $t = 24.0$ in (b) respectively. The reason of lack of signals in the early stage of Mode34 is that the wavelet signal is too small compared with that in the final stage when it amplifies rapidly. The first stage is characterized by the dominant wavenumber of each disturbance mode, m=4 and 18 for (a) and (b), respectively. However, no sooner than the stability phase transition occurs to the tertiary instability, component of higher azimuthal wavenumber break out abruptly. Even in the tertiary instability regime, Mode01 keeps $\pi/2$[rad] rotational symmetry in the circumferential direction. On the other hand, the wavelet signal of Mode34 which have non-uniform distribution of intensity begins to merge into groups (at $t = 23$) before the apparent tertiary instability, and finally, vortices are concentrated in 2 azimuthal areas in the tertiary instability regime. Notable is that rotationally asymmetric mode as Mode34 shows qualitatively different evolution, compared with symmetric one.

Fourier analysis gives another aspect of this local concentration found in Mode34. The temporal development of typical azimuthal Fourier modes of ω_z is shown in Fig.6 which are measured on the circle of $r = D/2$ in the cross-section S which moves to downstream as time goes on. The wavenumber $m = 1$ which corresponds to the circumferential asymmetry of Mode34 develops with second biggest spectrum density after the fundamental one of $m = 18$. This may be the key process how the modulation and the concentration of streamwise vortices happens. Spectrum densities of other Fourier modes increase abruptly at $t = 23$, exactly the same moment when the wavelet signal begins to concentrate to 2 areas shown in Fig.5(b). So, these modes are considered to be the higher wavenumber components induced by the infinitesimal distortion of the baseflow. Inferring the linear bound of the secondary instability of Mode34 on the basis of Fig.4, it is at around $t = 26$ since Mode34 is kept linear up to $t \simeq 26$. However, azimuthal Fourier modes in Fig.6 suggests that the disturbance already reached locally the linear bound of the secondary instability at $t \simeq 23$.

The mechanism of the temporal development of streamwise vortices is still unclear beyond the tertiary instability. However, above results suggests that small local non-uniformity induces local difference in receptivity of disturbance and this different receptivity amplifies successively at locally different growth rate of disturbances.

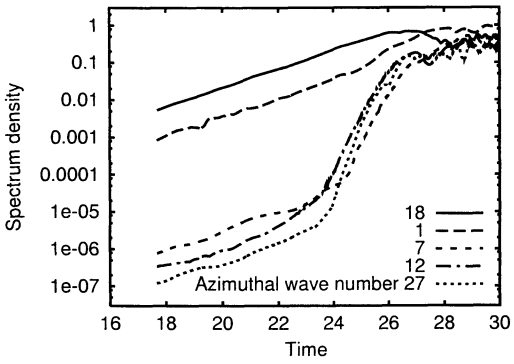

Figure 6: Temporal evolution of typical azimuthal Fourier modes when Mode34 is applied at t=17.5.

Since not a small difference lying between eigenvalues of Mode01 and 34, the mode of largest growth rate might dominate in the secondary instability in a braid region. However, in both temporal and spatial evolution of the secondary instability stage, local non-uniformity along circumference is found and disturbed field is assumed to be composed of various modes which triggers manifestation of non-linear interaction in early evolutional stage. Mode34 is one of such modes. If streamwise vortices in the braid region were always rotationally symmetric, it would be possible to predict their development such as the distance of virtual origin without big scatter. However, it is normal to assume that disturbances contains modes which triggers non-linearity. Then, even a small disturbance of this sort may modulate the evolution process. So, it is intrinsically unavoidable to have scatter of evolution speed of a round jet.

A BRAID REGION IN A SPATIALLY DEVELOPING JET

The unstable modes in a braid region of a temporally developing jet have been described in the last few sections. Now, it is intended here to consider the streamwise vortical structure in the braid of a practical spatially developing jets (Takeuchi et al, 1999) to see how above-mentioned secondary instability behaves.

In order to implement the role of unstable modes in spatial developing process, two-dimensional velocity and pressure field in the central cross-section of Mode34 in Fig.2(f) is introduced as a typical unstable mode at the nozzle exit. This disturbance is continuously

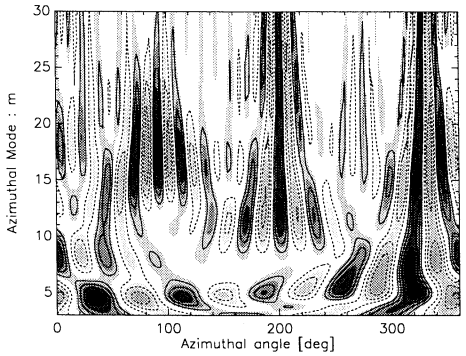

Figure 7: Wavelet maps of ω_z in the spatially evolving jet, measured at $z = 4.8$ in the braid region.

superposed on the mean velocity profile and no other random disturbances are assumed, to see the dependence of developed streamwise vortices in a cross section S on the mode and its spatial development. In the present simulation, the intensity of the supplied plane disturbance is $0.0001U_0$.

Fig.7 is the wavelet map of the distribution of ω_z along a circle of radius $r = D/2$ in the cross section at $z = 4.8$ after sufficient time from the introduction of the plane mode of Mode34. Near the band $m = 18$ in Fig.7, there remains the wavelet signal which probably comes from Mode34 superposed at the nozzle exit, and in the higher band of wavenumber space the strong signal concentrates in 3 or 4 azimuthal positions which is different from the temporal evolution of Mode34 demonstrated in Fig.5. The signal found in the band $m=4 \sim 6$ may be the components of more unstable modes, such as Mode01 and 04 in Fig.2, since they have the similar number of streamwise structures in the circumferential direction. This indicates that the highly unstable modes such as Mode01,02, etc., can be introduced in a braid region by the feedback process from turbulent vortical structures in the downstream chaotic region through the pressure disturbance, even though an unstable mode of smaller eigenvalue only is superposed on the mean velocity at the nozzle exit. As a result, the temporal increase of I measured in a braid of a spatially evolving jet is as fast as Mode01(Takeuchi, 2001), irrespective of the mode specified at the nozzle exit.

Accordingly, above results suggests that the secondary instability in a braid of a spatially evolving jet is characterized by diversity of local receptivity of disturbance, and the development of disturbances in the braid region can be attributed to the mechanism obtained by the global instability analysis.

CONCLUSIONS

The early stage of transition to turbulence of a round jet is investigated by analyzing the evolution of disturbances in the braid region between two neighbouring vortex rings. Global stability analysis and wavelet transform enable us to understand the physics of the phenomenon of the decay process of round jet. Major conclusions are as follows.

1. Eigenvalues of secondary instability for the braid region of a temporally developing jet has no dominant mode.

2. These modes grows linearly in the linear regime which is independent on the mode, but the growth rate depends strongly on the mode beyond the linear bound.

3. Mode having rotationally asymmetric eigenvector plays crucial role to induce three-dimensionality and accordingly nonlinearity of instability. This is reflected as non-uniform receptivity of disturbances in azimuthal direction.

4. In a practical spatially developing round jet, azimuthal non-uniformity of growth of disturbances characterizes the early stage of randomization whose mechanism can be attributed to that investigated in the temporally developing jet.

REFERENCES

Arnoldi,W.E., 1951, "The principle of Minimized Iterations in the Solution of the Matrix Eigenvalue Problem", *Quart.Appl.Math.9*,**9** pp.17–29

Chui,C.K., 1992, "An Introduction to Wavelets", ACADEMIC PRESS Inc., Orland, Florida

Eriksson,L.E. and Rizzi,A., 1985, "Computer-Aided Analysis of the Convergence to Steady State of Discrete Approximation to the Euler Equations", *J.Comp.Phys.*, **57** pp.90–128

Liepmann,D. and Gharib,M., 1992, "The role of streamwise vorticity in the near-field entrainment of round jets", *J. Fluid Mech.*, **245** pp.643–668

Saad,Y., "Variations on Arnoldi's Method for Computing Eigenelements of Large Unsymmetric Matrices" *Linear Algebra and Its Applications*, **34** (1980) pp.269–295

Takeuchi,S., 2001, "Analysis of a Decay Process in a Round Jet by a Direct Numerical Simulation", Ph.D. Thesis, Graduate School of Eng., Osaka Univ., Osaka, Japan

Takeuchi,S., Miyake,Y. and Kajishima,T., 1999, "On the Numerical Simulation of Round Jets of Imcompressible Fluid", *Proc. of 3rd ASME/JSME Joint Fluids Eng.Conf.* paper No.6957